# Temperature dependence of self-pulsation in compact disc lasers

S.A. Lynch, P. McEvoy, J. O'Gorman, P. Rees, W. Elsäßer and P. Landais

**Abstract:** Experimental data regarding the temperature dependence of compact disc lasers are presented. The authors demonstrate, for the first time, a temperature-dependent model which has been adapted from a well established compact disc laser model. By comparing the experimental trends and calculation, they attempt to highlight the role of certain phenomena such as non-radiative recombination and charge carrier diffusion on the device behaviour. From these results they come to a number of important conclusions regarding the origin of self-pulsation in these types of laser diodes.

## 1 Introduction

Self-pulsation is the term commonly used to describe the pulsed optical emission obtained from certain laser diodes when operated under DC bias. Since the advent of the very first semiconductor lasers, self-pulsation has been observed, and was originally considered as an undesirable phenomenon associated with degraded devices, [1–4]. Due to progress in epitaxial growth technology, defect induced self-pulsation is only rarely observed in newly manufactured components.

In more recent years it has been realised that self-pulsation can be highly advantageous in some applications. For example self-pulsation has been intensively studied for potential applications such as clock recovery in telecommunications systems, since it has been demonstrated that lasers which self-pulsate can be synchronised to the clock frequency of a return to zero encoded optical data stream [5, 6]. However, the most widespread use of self-pulsating lasers today is in optical data storage systems such as the compact disc player. This is because self-pulsating lasers have very low relative intensity noise characteristics, since their short coherence length makes them less sensitive to optical feedback.

The conventional compact disc laser diode is a narrow stripe component (Fig. 1). The laser diodes are designed so that the lateral electromagnetic field extends from an electrically pumped region of the stripe layer, to unpumped regions on either side, which act as saturable absorber sections. Self-pulsation results from the interaction of the confined electromagnetic field with this non-uniformly pumped material. By varying the heatsink temperature, $T$, in a range from 77 K to 370 K, we change fundamental material characteristics such as the material gain, charge carrier recombination rates and charge carrier diffusion rates. By also incorporating these variations into a simple rate equation model we can assess the impact of these parameters on the self-pulsating behaviour.

## 2 Experimental investigation

### 2.1 Experimental set-up

We tested four Sharp LT022MD laser diodes over a wide range of operating conditions and found that the behaviour of each device was very similar. As far as possible we have tried to present the experimental trends from one representative device, in order to preserve some element of consistency. A transverse cross-section showing the epitaxial layer structure of the laser diodes is shown in the inset of Fig. 1. The laser consists of a Fabry-Perot cavity defined by cleaved facets. The active region is bulk AlGaAs with emission wavelength $\lambda = 800$ nm. The gain section is pumped through a p-type electrical contact and has the following approximate dimensions: 250 μm long, 2 μm wide and 0.2 μm thick. The two n-blocking layers confine the current to the central region of the active layer, resulting in two lateral unpumped regions at the sides which act as saturable absorber regions. The optical mode propagating along the cavity overlaps these regions.

As illustrated in Fig. 1, this component is placed in a liquid nitrogen cryostat which allows a temperature tuning in the range from 77 K to 370 K. The emitted light is collected by a 0.65 NA microscope objective and passes an 36 dB optical isolator, to avoid any feedback which could influence the self-pulsating behaviour. At the isolator output the light is monitored by an integrating sphere (not shown in Fig. 1) or a 60 GHz photodiode to transform the optical output to an electrical signal. The converted electrical signal is observed with a 22 GHz bandwidth spectrum analyser (HP 8563A). A typical RF spectrum of a self-pulsating laser is shown in Fig. 2. The spectrum is characterised by a main peak at 1.03 GHz which corresponds to the self-pulsation



*IEE Proceedings* online no. 20040792

doi: 10.1049/ip-opt:20040792

Paper received 29th October 2003. Originally published online 29th November 2004

S.A. Lynch is with the Semiconductor Physics Group, Cavendish Laboratory, University of Cambridge, Cambridge CB30HE, UK

P. McEvoy is with The Technology Partnership, Melbourn Science Park, Royston, Herts SG8 6EE, UK

J. O'Gorman is with Eblana Photonics, Trinity College Enterprise Centre, Pearse Street, Dublin 2 Ireland

P. Rees is with the School of Informatics, University of Wales, Bangor LL57 1UT, UK

W. Elsäßer is with the Institut für Angewandte Physik, Technische Universität Darmstadt, Schlossgartenstr. 7, D-64289 Darmstadt, Germany

P. Landais is with the School of Electronic Engineering, Dublin City University, Glasnevin 9, Ireland

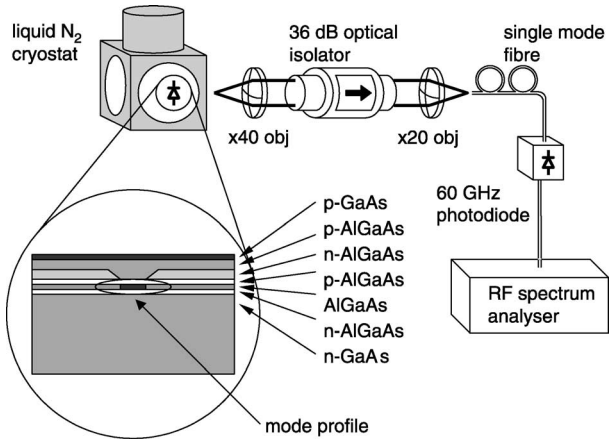


**Fig. 1** *Schematic of experimental set-up*
Inset shows the structure of the self-pulsating CD laser

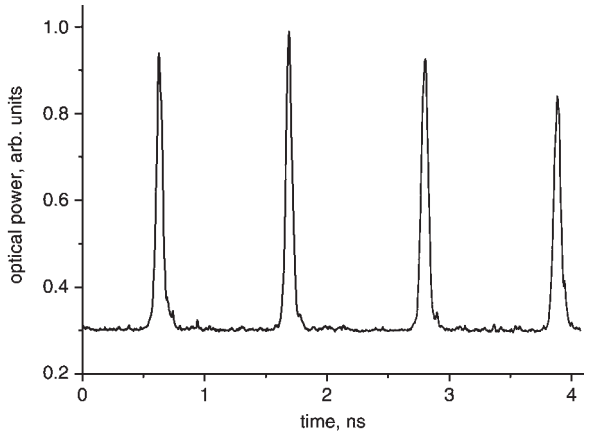


**Fig. 3** *Plot of the optical power as a function of time for a typical Sharp LT022MD laser diode*
NB This was not the same laser used in the other Figures
In this case the bias current was 46 mA at a heatsink temperature of 25 °C

frequency $v_{sp}$. The following peaks at 2.07, 3.10, 4.14 and 5.18 GHz are higher-order harmonics.

Figure 3 shows a time trace of the emitted optical power recorded on a streak camera. In order to avoid perturbing the free-running self-pulsating dynamics of the laser diode, the streak camera was run in single shot mode. This meant that it was not necessary to apply a synchronising electrical modulation to the laser diode which would be necessary as a trigger for synchroscan mode. Figure 3 shows a 4 ns streak in which four pulses were recorded. The Figure shows that the laser under test has a free cycle of approximately 10%.

## 2.2 Experimental results

Figure 4 shows a semi-logarithmic plot of threshold current against $T$. This plot can be used to determine the characteristic temperature, $T_0$:

$$I_{th} = I_0 \exp\left(\frac{T}{T_0}\right) \quad (1)$$

where $I_{th}$ is the threshold current and $I_0$ is the $y$-axis intercept. $T_0$ describes the sensitivity of the threshold current to the temperature. Light/current curves were recorded at 20 K intervals for a temperature range from 77 K to 370 K and the corresponding threshold currents were measured. As the temperature increases the peak gain at a given carrier density is reduced requiring a higher bias current to achieve the lasing threshold. Furthermore, since there is an additional Joule heating effect associated with the increased current, nonradiative effects in recombination further add to the escalation in the laser threshold current. The typical temperature-dependent threshold behaviour for AlGaAs laser diodes is usually well described by (1) according to [7, 8]. For the data shown in Fig. 4, when fitted to the exponential form described by (1), $T_0$ can be seen to change continuously over the temperature range in question. For example, around 100 K $T_0 = 85$ K, but at room temperatures $T_0 = 184$ K.

As shown in Figure 5, these data are re-plotted on a double-logarithmic axis. The highly linear curve, over most of the measured range indicates a power law dependence. It can be shown, assuming the losses in the laser are temperature independent, that the threshold current, $I_{th}$, should scale as $T^{d/2}$ where $d$ is the dimensions of the gain medium [9, 10]. For bulk active regions, $d$ is equal to three, for a quantum well it is equal to two, for quantum wires it is one, and for quantum dots zero. Thus, for an ideal bulk active region $I_{th}$ is proportional to $T^{1.5}$ and for an ideal quantum well active region $I_{th}$ is proportional to $T$. The slope of the curve in Fig. 5 was found to be 1.3, indicating

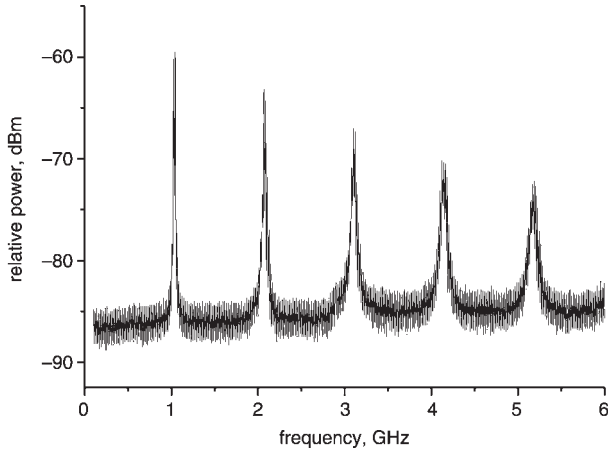


**Fig. 2** *Typical RF spectrum for a commercial Sharp LT022MD SP CD laser diode recorded at a bias current of 50 mA and a heatsink temperature of 20 °C*
The resolution bandwidth of the RF spectrum analyser was 1 MHz and the video bandwidth was 3 kHz

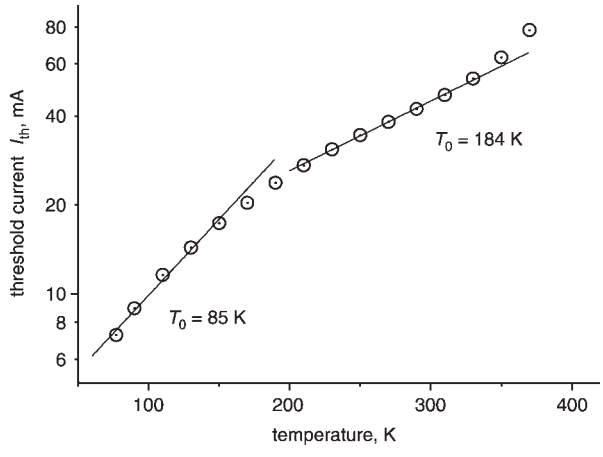


**Fig. 4** *Semi-logarithmic plot of experimentally measured $I_{th}$ against temperature*
Two values of $T_0$ are shown at different extremes of temperature

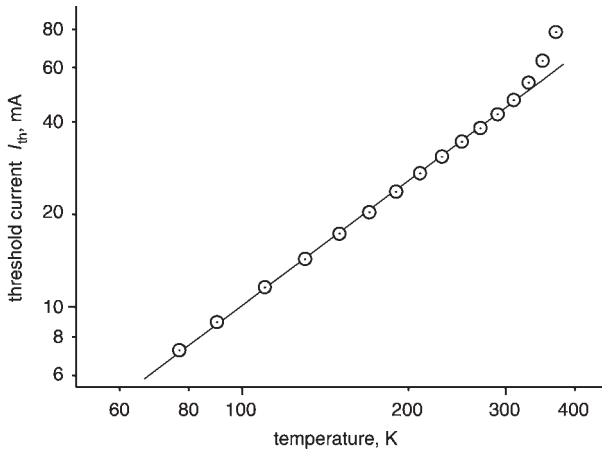


**Fig. 5** *Double-logarithmic plot of experimentally measured $I_{th}$ against temperature*

that the gain medium shows predominantly bulk characteristics. As the temperature increases, the thermal energy allows the carriers to recombine non-radiatively to higher minima in the band structure of the AlGaAs. The carriers do not contribute to the radiative recombination. This explanation is justified by the fact that for any molar fraction of Al above approximately 0.35, the semiconductor material becomes indirect [11].

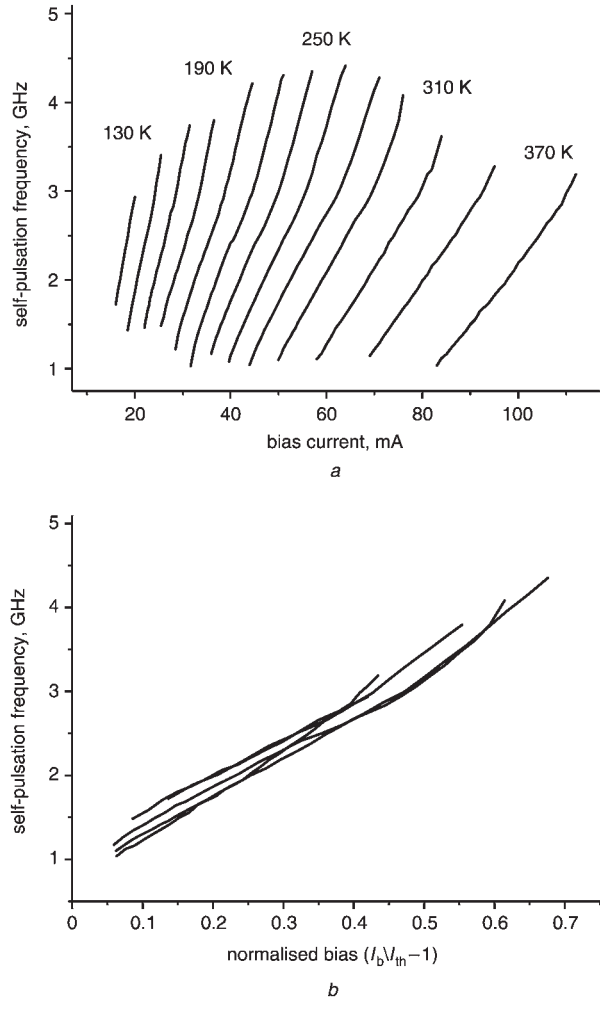


**Fig. 6** *Experimentally measured self-pulsation frequency*
*a* Self-pulsation frequency against bias current
*b* Self-pulsation frequency against normalised bias current

Figure 6*a* shows the self-pulsation frequency as a function of bias current for several temperatures in a range from 110 K to 370 K. Self-pulsation was found to extinguish around $T = 100$ K. The upper limit of 370 K is determined by the packaging and is not the upper temperature at which self-pulsation is found to extinguish. The relationship between the self-pulsation frequency and the bias current is linear and is more sensitive to changes in the bias current at lower temperatures. Previously a nonlinear behaviour has been observed, but for this study, the focus was on the dependence of the self-pulsation with the bias current in the vicinity of the threshold current [12]. In Fig. 6*b*, the self-pulsating frequency is re-plotted as function of normalised bias current. It is clear that these curves do not follow the simple square root rule observed for relaxation oscillations [7, 13]. To achieve a deeper understanding, we have developed a model based on rate equations.

## 3 Calculation

### 3.1 Rate equation model

We use a set of single-mode rate equations [14–17] describing the evolution of the photon number, $P$, and carrier numbers, $N_i$. The subscript $i = 1$ ($i = 2$) is related to the gain (saturable absorber) section. Owing to the symmetric nature of the laser geometry the saturable absorber sections on both sides of the gain section are described in the rate equations as a single lumped section with an associated lumped carrier number, $N_2$. The model assumes that both the gain and absorber sections show no spatial variation in carrier density or photon density, other than that existing at the boundary between sections. Our model may be written as:

$$\frac{dN_1}{dt} = \frac{I_b}{e} - \gamma_{e1}(N_1, T)N_1 - \Gamma_1(N_1, T)G(N_1, T)P - \frac{N_1 - N_2}{\tau_{12}(N_1, T)} \tag{2}$$

$$\frac{dN_2}{dt} = -\gamma_{e2}(N_2, T)N_2 - \Gamma_2(N_2, T)G(N_2, T)P - \frac{N_2 - N_1}{\tau_{21}(N_2, T)} \tag{3}$$

$$\frac{dP}{dt} = \left[\sum_{i=1}^{2} \Gamma_i(N_i, T)G(N_i, T) - \frac{1}{\tau_p}\right]P + \beta \sum_{i=1}^{2} B(N_i, T)N_i^2 \tag{4}$$

where $\Gamma_i$ is the confinement factor and is discussed further on. $\beta$ represents the coupling efficiency of the spontaneous emission to the lasing mode, $B(N_i, T)$ the bimolecular recombination rate. $I_b$ is the injection current into the gain section, and $e$ the electron charge. $G$ is the gain or absorption in the active layer, and $\tau_p$ the photon lifetime given by:

$$\tau_p^{-1} = v_g\left[\alpha_{int} + \frac{1}{L}\ln\left(\frac{1}{R}\right)\right] \tag{5}$$

where $v_g$ is the group velocity, $\alpha_{int}$ the internal losses, $L$ the cavity length, and $R$ the reflectivity of the output mirrors. The carrier recombination rate, $\gamma_{ei}(N_i, T)$ is expressed as:

$$\gamma_{ei}(N_i, T) = A(N_i, T) + B(N_i, T)N_i \tag{6}$$

where $A(N_i, T)$ is the non-radiative recombination rate. A quadratic Auger recombination term has not been taken into account in our model since it is considered negligible in materials with large band-gaps. $\tau_{12}$ is the charge carrier diffusion time from section 1 to section 2 given by:

$$\tau_{12} = \frac{\omega^2}{2D} \tag{7}$$

where $\omega$ is the width of the gain section and $D$, the diffusion coefficient is defined by the Einstein relation:

$$D = 2\mu(T)k_b T\left[e\left(\frac{m_h}{m_e}+1\right)\right]^{-1} \tag{8}$$

where $\mu(T)$ is the electron mobility, $k_b$, Boltzmann's constant and $m_e$, $m_h$ the respective effective masses of the electron and hole. We used experimental data obtained from the literature to quantify the variation of $\mu(T)$ with temperature [18]. The ambipolar carrier diffusion time from Section 1 to Section 2, $\tau_{12}$, is related to its counterpart for diffusion from Section 2 to Section 1, $\tau_{21}$, by the relation:

$$\tau_{12} = \left(\frac{V_1}{V_2}\right)\tau_{21} \tag{9}$$

where $V_i$ is the volume of the section $i$. The parameters used in (2)–(4) are listed in Table 1. We numerically solve the equation set (2)–(4) using a 0.1 ps time step Runge-Kutta method of the fifth-order. The dynamic response has been calculated as a function of $I_b$ over the temperature range. For each temperature and bias current, we extracted the self-pulsation frequency, by performing a Fourier analysis on the pulse train over a large number of pulses. Before analysing the results, we must clarify the temperature dependence of the parameters listed in (2)–(4).

## 3.2 Temperature dependence

We incorporate the effect of temperature on material gain and absorption. The temperature change is also assumed to affect the confinement factor and the carrier lifetime through their dependence on carrier density and through the recombination parameters. Charge carrier diffusion is considered to vary according to (8), which includes the temperature dependence of the electron mobility. The following Sections describe the temperature dependence of the parameters listed in Table 1 and used in our model.

### 3.2.1 Gain and absorption in the material:

The peak gain is pre-calculated as a function of carrier density and temperature and is included in the laser model using two-dimensional interpolation. A parabolic band structure is assumed for the light and heavy hole valence bands, $\gamma$, X and $L$ minima of the conduction band. The electron and hole Fermi functions $f_c$ and $f_v$ are obtained by imposing the charge neutrality condition in the undoped active region. Stating a strict $k$-selection the gain/absorption coefficient and spontaneous emission rate [7, 8] are given by (10) and (11). The value of $B(N_i, T)$ is then obtained by integrating $r_{sp}(\hbar\omega)$ over the spectral energy range $E_{eh}$, while due to the standard convention for rate equation models the gain is taken at the local maximum of the gain spectrum:

$$\alpha(\hbar\omega) = \int \frac{e^2 h}{2\epsilon_0 m_0^2 c n_g(\hbar\omega)}|M_b|^2\rho_{red}(\hbar\omega) \times [1 - f_c - f_v]L(E_{eh}, \hbar\omega)dE_{eh} \tag{10}$$

$$r_{sp}(\hbar\omega) = \int \frac{4\pi n_g e^2(\hbar\omega)}{\epsilon_0 m_0^2 c^3 h^2}|M_b|^2\rho_{red}(\hbar\omega) \times f_c f_v L(E_{eh}, \hbar\omega)dE_{eh} \tag{11}$$

$\rho_{red}(\hbar\omega)$ is the three-dimensional reduced density of states and $|M_b|^2$ is the Kane matrix element [7, 8]. The many-body effects include bandgap renormalisation and spectral broadening and are included phenomenologically. Spectral broadening due to carrier–carrier scattering is described using the Lorentzian convolution given by:

**Table 1: Parameters used in our model and their temperature dependence**

| Parameters | Symbol | Unit | Value in temperature range 77 K ≤ $T$ ≤ 310 K |
|---|---|---|---|
| Non-radiative recombination rate for the gain section | $A(N_1, T)$ | $s^{-1}$ | in the range $10^8 \le A(N_1, T) \le 5\times10^8$ |
| Non-radiative recombination rate for the SA section | $A(N_2, T)$ | $s^{-1}$ | in the range $10^8 \le A(N_2, T) \le 5\times10^8$ |
| Radiative recombination rate for the gain section | $B(N_1, T)$ | $s^{-1}$ | calculated from the gain model but typically $5\times10^8 \le B(N_1, T) \le 1.5\times10^9$ |
| Radiative recombination rate for the SA section | $B(N_2, T)$ | $s^{-1}$ | calculated from the gain model but typically $5\times10^8 \le B(N_2, T) \le 1.5\times10^9$ |
| Thickness of the active layer | $d$ | μm | 0.2 |
| Length of component | $L$ | μm | 250 |
| Width of active layer | $W$ | μm | 2 |
| Effective hole mass | $m_h$ | | 0.63 |
| Effective electron mass | $m_e$ | | 0.078 |
| Mobility | $\mu$ | $cm^2(Vs)^{-1}$ | in the range $10^6 \le \mu \le 5\times10^3$ |
| Reflection coefficient of the facet | $R$ | | 0.3 |
| Group refractive index of active layer | $n_g$ | | 3.5 |
| Group velocity | $v_g$ | $cms^{-1}$ | $8.6\times10^9$ |
| Spontaneous emission coupling factor | $\beta$ | | $10^{-5}$ |
| Internal losses | $\alpha_{int}$ | $cm^{-1}$ | 10 |

$$L(E_{eh}, \hbar\omega) = \frac{1}{\pi}\left[\frac{(\hbar/\tau_{in})}{(E_{eh} - \hbar\omega)^2 + (\hbar/\tau_{in})^2}\right] \quad (12)$$

with a weakly carrier-concentration-dependent scattering lifetime [19], of the form:

$$\tau_{in} = 1 \times 10^{-8}\left[2\left(\frac{n_i}{V_i}\right)^{-\frac{1}{3}}\right] \quad (13)$$

where dimensions of $cm^{-3}$ for $n_i$, the carrier density, and $cm^3$ for $V_i$, and a pre-factor of $1 \times 10^{-8}$ result in dimensions of $s^{-1}$ for the scattering lifetime. The bandgap renormalisation [7], is included as a rigid reduction $\Delta E$ (in eV), in the effective band gap:

$$\Delta E = 1.6 \times 10^{-8}\left[2\left(\frac{n_i}{V_i}\right)^{\frac{1}{3}}\right] \quad (14)$$

The peak gain, defined at the local maximum of the gain against wavelength curve is then calculated as a function of carrier density. Figure 7 shows the calculated variation of peak gain with carrier density for five different temperatures between 100 K and 300 K. The calculated gain presents an usual temperature and carrier dependence. This gain model has already been used to successfully predict the gain and spontaneous emission as a function of temperature in both GaAs and GaInP bulk lasers [20].

Our representation of the many-body effects in our model has two advantages. Firstly this calculation results in more realistic values for the gain, the absorption, and their temperature dependence, rather than the common assumption that the gain is a linear function of the carriers. Secondly the gain calculation introduces a self-consistency in the model, since the radiative recombination rates for each section, from which the carrier recombination rates and spontaneous emission rates are calculated, are now determined by only one calculation.

### 3.2.2 Carrier recombination rate and carrier diffusion:

The non-radiative recombination rate increases as the temperature increases [21], however, given the uncertainty in the literature of the temperature dependence of $A$, we assume a linear relationship as a first approximation. The radiative recombination rate is determined along with the laser gain as shown in (11). The total carrier recombination rate is then achieved using (6).

The temperature dependence of the charge carrier diffusion is calculated using (8). Temperature enters this equation both explicitly and implicitly through the highly nonlinear temperature dependence of the mobility. Mobilities were estimated using experimental data from [18], and were increased by over two orders of magnitude for the lower temperatures. Table 1 summarises the parameters used in our model and indicates their variation with temperature.

### 3.2.3 Confinement factor $\Gamma$:

The confinement of the optical field, $\Gamma$ is defined as the overlap of the optical mode and the active region. The variation of the carrier density affects $\Gamma$ through both changes along the TE mode in the refractive index and the gain/absorption of the active layer. If this factor changes, the interaction between the optical power and the active layer is modified. This has an impact on the pulsation dynamics since the carrier number of the gain and SA sections varies during pulse formation and emission. For each time step, we calculate the TE mode distribution using the approach described in [14]. In the present model, the carrier mobility, the gain, the carrier recombination factors and the spontaneous emission rate are carrier and/or temperature dependent as shown in Table 1. The refractive index variation is a function of the carrier number as given in [12]. Since the carrier number is temperature dependent it is possible to draw a temperature dependence for the confinement factor. The shape of the optical mode is calculated by solving the electric field distribution in the plane parallel to the facets. The confinement factors are then used in the solution of (2)–(4).

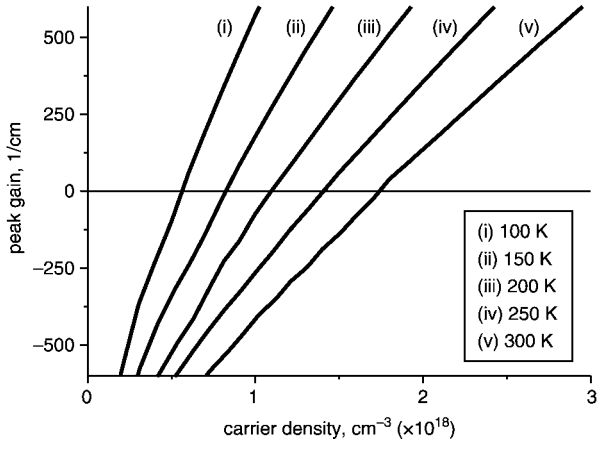


**Fig. 7** *Calculated peak gain against carrier density for five different temperatures*

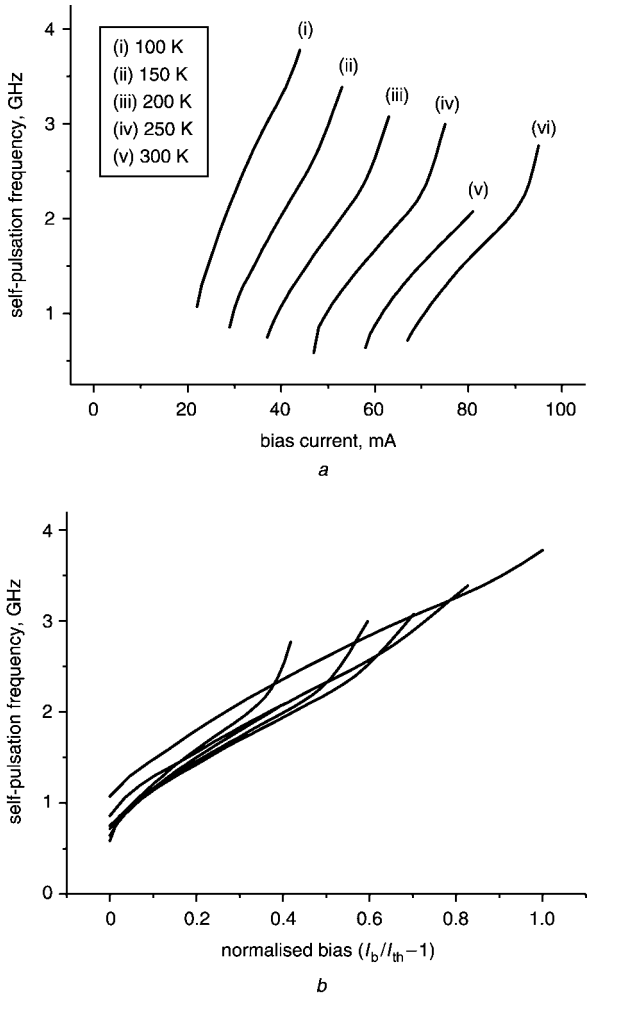


**Fig. 8** *Calculated self-pulsation frequency*

*a* Self-pulsation frequency against bias current
*b* Self-pulsation frequency against normalised bias current

### 3.3 Calculated results and discussion

With the model described above, we investigated the behaviour of a CD laser over a similar range of temperature and current than that described in Section 2. Figure 8*a* shows the variation of self-pulsation frequency with bias current for several temperatures, and should be compared with Fig. 6*a*. As already shown previously in the Section 2 for a given temperature, as the current increases the frequency increases monotonously. As the temperature increases, more current is required to keep the self-pulsation frequency at a constant value. See in Figs. 8*b* and 6*b*, that the normalised current increases the value of the self-pulsation frequency independently from the temperature condition. By presenting the self-pulsation as a function of the normalised current, the effects due to the gain variation on the self-pulsation are highlighted. If any gain changes were influential on the self-pulsation behaviour, the self-pulsation frequency curve would not have been superimposed. Therefore, the self-pulsation is not driven by the gain and absorption balance of the cavity. Furthermore, the carrier diffusion varying drastically with temperature affects both the gain and the absorption, this is not observed on the normalised curves. Hence, the impact of the carrier diffusion is not direct on the self-pulsation frequency value.

## 4 Conclusions

We have presented experimental and simulated investigations on the temperature dependence of self-pulsation in CD laser diodes. We have described a rate equation model that includes temperature, and show it to accurately predict the behaviour of this type of laser diode over a wide range of operating temperatures. We have presented experimental data on the temperature dependence of threshold current and explain the deviation from the usual exponential form using a simple recombination model. We conclude from this that non-radiative recombination does not play a significant role in the behaviour of this type of laser diode. We have shown that the self-pulsation frequency is experimentally observed to vary linearly with normalised bias current and that the gradient of these curves is highly temperature independent. This behaviour is also reflected in the simulated data from our model. From this we conclude that charge carrier diffusion does not play a first-order role in driving the self-pulsation. These observations suggest that it is an over-simplification to describe self-pulsation in CD lasers as just a destabilised relaxation oscillation, and that the physics behind this phenomenon is considerably more complicated.

## 5 Acknowledgments

The authors thank Prof. Peter Blood, Department of Physics and Astronomy, Cardiff University, for fruitful discussions.

During the time of this research, Pascal Landais was supported by the EU commission under the Training and Mobility of Researchers programme. Stephen A. Lynch and Paul McEvoy were partially funded by Enterprise Ireland research scholarships.

## 6 References

1 Basov, N.G.: 'Dynamics of injection lasers', *IEEE J. Quantum Electron.*, 1968, **4**, pp. 855–867
2 Yang, E.S., McMullin, P.G., Smith, A.W., Blum, J., and Shih, K.K.: 'Degradation induced microwave oscillations in double-heterostructure lasers', *Appl. Phys. Lett.*, 1974, **2**, pp. 324–326
3 Van der Ziel, J.P., Merz, J.L., and Paoli, T.L.: 'Study of intensity pulsations in proton-bombarded stripe-geometry double-heterostructure AlGaAs lasers', *J. Appl. Phys.*, 1979, **50**, (7), pp. 4620–4637
4 Ueno, M., and Lang, R.: 'Conditions for self-sustained pulsation and bistability in semiconductor lasers', *J. Appl. Phys.*, 1985, **58**, pp. 1689–1692
5 Jinno, M., and Matsumoto, T.: 'Nonlinear operations of 1.55 μm wavelength multielectrode distributed-feedback laser diodes and their applications for optical signal processing', *J. Lightwave Technol.*, 1992, **29**, pp. 448–457
6 Duan, G.-H., and Pham, G.: 'Injection-locking properties of self-pulsation in semiconductor lasers', *IEE Proc., Optoelectron.*, 1997, **144**, pp. 228–234
7 Agrawal, G.P., and Dutta, N.K.: 'Long-wavelength semiconductor lasers' (Van Nostrand Reinhold, New York, NY, USA, 1986)
8 Coldren, L.A., and Corzine, S.W.: 'Diode lasers and photonic integrated circuits' (Wiley, 1995)
9 Blood, P., Fletcher, E.D., Woodbridge, K., Heasman, K., and Adams, A.: 'Influence of the barriers on the temperature dependence of threshold current in GaAs/AlGaAs quantum well lasers', *IEEE J. Quantum Electron.*, 1989, **25**, (6), pp. 1459–1468
10 Landsberg, P.T.: 'Recombination in semiconductors' (Cambridge University Press, Cambridge, UK, 1991)
11 Kapon, E.: 'Semiconductor laser II Materials and strucures' (Academic Press, 1999)
12 Mirasso, C.R., van Tartwijk, G.H.M., Hernndez-Garca, E., Lenstra, D., Lynch, S., Landais, P., Phelan, P., O'Gorman, J., San Miguel, M., and Elser, W.: 'Self-pulsating semiconductor lasers: Theory and experiment', *IEEE J. Quantum Electron.*, 1999, **35**, (5), pp. 764–770
13 Buus, J.: 'Comparison of two recent semiconductor laser models', *IEEE J. Quantum Electron.*, 1983, **19**, (9), pp. 1356–1358
14 Yamada, M.: 'A theoretical analysis of self-sustained pulsation phenomena in narrow stripe semiconductor lasers', *IEEE J. Quantum. Electron.*, 1993, **29**, pp. 1330–1336
15 Lasher, G.J.: 'Analysis of a proposed bistable injection laser', *Solid-State Electron.*, 1964, **7**, pp. 707–716
16 Avrutin, E.A.: 'Analysis of spontaneous emmision and noise in self-pulsing laser diodes', *IEE Proc. J, Optoelectron.*, 1993, **140**, pp. 16–20
17 Duan, G.H., Landais, P., and Jacquet, J.: 'Modeling and measurement of bistable semiconductor lasers', *IEEE J. Quantum Electron.*, 1994, **30**, pp. 2507–2515
18 Hirakawa, H., and Sakaki, H.: 'Mobility of the two-dimensional electron gas at selectively doped n-type AlGaAs/GaAs heterojunctions with controlled electron concentrations', *Phys. Rev. B., Condens. Matter*, 1986, **33**, (12), pp. 8291–8303
19 Blood, P., Colak, S., and Kucharska, A.I.: 'Influence of broadening and high injection effects on GaAs-AlGaAs quantum well lasers', *IEEE J. Quantum Electron.*, 1988, **24**, pp. 1593–1604
20 Rees, P., Summers, H., and Blood, P.: 'Gain current calculations for bulk GaInP lasers including many body effects', *Appl. Phys. Lett.*, 1991, **59**, (27), pp. 3521–3523
21 Gurioli, M., Vinattieri, A., Colocci, M., Deparis, C., Massies, J., Neu, G., Bosacchi, A., and Franchi, S.: 'Temperature dependence of the radiative and nonradiative recombination time in GaAs/AlGaAs quantum-well structures', *Phys. Rev., B., Condens. Matter Mater. Phys.*, 1991, **44**, (7), pp. 3115–3124